
Robustly overfitting latents for flexible neural image compression

Yura Perugachi-Diaz¹ Arwin Gansekoele² Sandjai Bhulai¹

Abstract

Neural image compression has made a great deal of progress. State-of-the-art models are based on variational autoencoders and are outperforming classical models. Neural compression models learn to encode an image into a quantized latent representation that can be efficiently sent to the decoder, which decodes the quantized latent into a reconstructed image. While these models have proven successful in practice, they lead to sub-optimal results due to imperfect optimization and limitations in the encoder and decoder capacity. Recent work shows how to use stochastic Gumbel annealing (SGA) to refine the latents of pre-trained neural image compression models. We extend this idea by introducing SGA+, which contains three different methods that build upon SGA. Further, we give a detailed analysis of our proposed methods, show how they improve performance, and show that they are less sensitive to hyperparameter choices. Besides, we show how each method can be extended to three- instead of two-class rounding. Finally, we show how refinement of the latents with our best-performing method improves the compression performance on the Tecnick dataset and how it can be deployed to partly move along the rate-distortion curve.

1. Introduction

Image compression allows efficient sending of an image between systems by reducing their size. There are two types of compression: lossless and lossy. Lossless image compression sends images perfectly without losing any quality and can thus be restored in their original format, such as the PNG format. Lossy compression, such as BPG (Bellard, 2014), JPEG (Wallace, 1992) or JPEG2000 (Skodras et al., 2001), loses some quality of the compressed image. Lossy compression aims to preserve as much of the quality of the

reconstructed image as possible, compared to its original format, while allowing a significantly larger reduction in required storage.

Traditional methods (Wallace, 1992; Skodras et al., 2001), especially lossless methods, can lead to limited compression ratios or degradation in quality. With the rise of deep learning, neural image compression is becoming a popular method (Theis et al., 2017; Toderici et al., 2017). In contrast with traditional methods, neural image compression methods have been shown to achieve higher compression ratios and less degradation in image quality (Ballé et al., 2018; Minnen et al., 2018; Lee et al., 2019). Additionally, neural compression techniques have shown improvements compared to traditional codecs for other data domains, such as video. (Agustsson et al., 2020; Habibian et al., 2019; Lu et al., 2019).

In practice, neural lossy compression methods have proven to be successful and achieve state-of-the-art performance (Ballé et al., 2018; Minnen et al., 2018; Lee et al., 2019). These models are frequently based on variational autoencoders (VAEs) with an encoder-decoder structure (Kingma & Welling, 2013). The models are trained to minimize the expected rate-distortion (R-D) cost: $R + \lambda D$. Intuitively, one learns a mapping that encodes an image into a compressible latent representation. The latent representation is sent to a decoder and is decoded into a reconstructed image. The aim is to train the compression model in such way that it finds a latent representation that represents the best trade-off between the length of the bitstream for an image and the quality of the reconstructed image. Even though these models have proven to be successful in practice, they do have limited capacity when it comes to optimization and generalization. For example, the encoder’s capacity is limited which makes the latent representation sub-optimal (Cremer et al., 2018). Recent work (Campos et al., 2019; Guo et al., 2020; Yang et al., 2020) proposes procedures to refine the encoder or latents, which lead to better compression performance. Furthermore, in neural video compression, other work focuses on adapting the encoder (Aytekin et al., 2018; Lu et al., 2020) or finetuning a full compression model after training to improve the video compression performance (van Rozendaal et al., 2021).

The advantage of refining latents (Campos et al., 2019; Yang

¹Vrije Universiteit Amsterdam, the Netherlands ²Centrum Wiskunde & Informatica, the Netherlands. Correspondence to: Yura Perugachi-Diaz <y.m.perugachidiaz@vu.nl>.

et al., 2020) is that improved compression results per image are achieved while the model does not need to be modified. Instead, the latent representations for each individual image undergo a refining procedure. This results in a latent representation that obtains an improved bitstream and image quality over its original state from the pre-trained model. As mentioned in (Yang et al., 2020), the refining procedure for stochastic rounding with Stochastic Gradient Gumbel Annealing (SGA) considerably improves performance. In this paper, we introduce SGA+, an extension of SGA that further improves compression performance and is less sensitive to hyperparameter choices. The main contributions are:

- We show how changing the probability space with more natural methods instead of SGA boosts the compression performance.
- We propose the sigmoid scaled logit (SSL), which can smoothly interpolate between the approximate atanh, linear, cosine and round. And we show how this function finds even better compression performance.
- We demonstrate a generalization to rounding to three classes, that contains the two classes as a special case.

Further, we show how SSL outperforms baselines on the Kodak dataset in terms of true loss curves. We show how our method generalizes to the Tecnick dataset in terms of peak signal-to-noise ratio (PSNR) versus the bits per pixel (BPP) in an R-D plot. In addition, we analyze the stability of all functions and show the effect of interpolation between different methods with SSL. Lastly, we propose a refining procedure at compression time that allows moving along the R-D curve when refining the latents with another λ than a pre-trained model is trained on. The code of our proposed methods will be published at a later time on GitHub.

2. Preliminaries and related work

In lossy compression, the aim is to find a mapping of image x where the distortion of the reconstructed image \hat{x} is as little as possible compared to the original one while using as little storage as possible. Therefore, training a lossy neural image compression model presents a trade-off between minimizing the length of the bitstream for an image and minimizing the distortion of the reconstructed image (Ballé et al., 2017; Lee et al., 2019; Minnen et al., 2018; Theis et al., 2017).

Neural image compression models from (Ballé et al., 2017; Minnen et al., 2018; Theis et al., 2017), also known as hyperpriors, accomplish this kind of mapping with latent variables. An image x is encoded onto a latent representation $y = g_a(x)$, where $g_a(\cdot)$ is the encoder. Next, y is

quantized $Q(y) = \hat{y}$ into a discrete variable that is sent losslessly to the decoder. The reconstructed image is given by: $\hat{x} = g_s(\hat{y})$, where $g_s(\cdot)$ represents the decoder. The rate-distortion objective that needs to be minimized for this specific problem is given by:

$$\begin{aligned} \mathcal{L} &= R + \lambda D \\ &= \underbrace{\mathbb{E}_{x \sim p_x} [-\log_2 p_{\hat{y}}(\hat{y})]}_{\text{rate}} + \lambda \underbrace{\mathbb{E}_{x \sim p_x} [d(x, \hat{x})]}_{\text{distortion}}, \quad (1) \end{aligned}$$

where λ is a Lagrange multiplier determining the rate-distortion trade-off, R is the expected bitstream length to encode \hat{y} and D is the metric to measure the distortion of the reconstructed image \hat{x} compared to the original one x . Specifically for the rate, p_x is the (unknown) image distribution and $p_{\hat{y}}$ represents the entropy model that is learned over the data distribution p_x . A frequently used distortion measure for $d(x, \hat{x})$, is the mean squared error (MSE) or PSNR.

In practice, the latent variable y often consists of multiple levels in neural compression. Namely, a smaller one named z , which is modeled with a relatively simple distribution $p(z)$, and a larger variable, which is modeled by a distribution for which the parameters are predicted with a neural network using z , the distribution $p(y|z)$. We typically combine these two variables into a single symbol y for brevity. Furthermore, a frequent method of quantizing $Q(\cdot)$ used to train hyperpriors consists of adding uniform noise to the latent variable.

2.1. Latent optimization

Neural image compression models have been trained over a huge set of images to find an optimal encoding. Yet, due to difficulties in optimization or due to constraints on the model capacity, model performance is sub-optimal. To overcome these issues, another type of optimizing compression performance is proposed in (Campos et al., 2019; Yang et al., 2020) where they show how to find better compression results by utilizing pre-trained networks and keeping the encoder and decoder fixed but only adapting the latents. In these methods, a latent variable y is iteratively adapted using differentiable operations at test time. The aim is to find a more optimal discrete latent representation \hat{y} . Therefore, the following minimization problem needs to be solved for an image x :

$$\arg \min_{\hat{y}} [-\log_2 p_{\hat{y}}(\hat{y}) + \lambda d(x, \hat{x})]. \quad (2)$$

This is a powerful method that can fit to a test image x directly without the need to further train an entire compression model.

2.2. Stochastic Gumbel Annealing

(Campos et al., 2019) proposes to optimize the latents by iteratively adding uniform noise and updating its latents. While this method proves to be effective, there is still a difference between the true rate-distortion loss ($\hat{\mathcal{L}}$) for the method and its discrete representation \hat{y} . This difference is also known as the discretization gap. Therefore, (Yang et al., 2020) propose the SGA method to optimize latents and show how it obtains a smaller discretization gap. SGA is a soft-to-hard quantization method that quantizes a continuous variable v into the discrete representation for which gradients can be computed. A variable v is quantized as follows. First, a vector $\mathbf{v}_r = (\lfloor v \rfloor, \lceil v \rceil)$ is created that stacks the floor and ceil of the variable, also indicating the rounding direction. Next, the variable v is centered between $(0, 1)$ where for the flooring: $v_L = v - \lfloor v \rfloor$ and ceiling: $v_R = \lceil v \rceil - v$. With a temperature rate $\tau \in (0, 1)$, that is decreasing over time, this variable determines the soft-to-hardness where 1 indicates training with a fully continuous variable v and 0 indicates training while fully rounding variable v . To obtain unnormalized log probabilities, the inverse hyperbolic tangent (atanh) function is used as follows:

$$\log(\pi) = (-\operatorname{atanh}(v_L)/\tau, -\operatorname{atanh}(v_R)/\tau). \quad (3)$$

Next, samples are drawn: $\mathbf{y} \sim \text{Gumbel-Softmax}(\pi, \tau)$ (Jang et al., 2016) and are multiplied and summed with the vector \mathbf{v}_r to obtain the quantized representation: $\hat{v} = \sum_i (v_{r,i} * y_i)$. As SGA aids the discretization gap, this method may not have optimal performance and may not be as robust to changes in its temperature rate τ .

Besides SGA, (Yang et al., 2020) propose deterministic annealing (Agustsson et al., 2017), which follows almost the same procedure as SGA, but instead of sampling stochastically from the Gumbel Softmax, this method uses a deterministic approach by computing probabilities with the Softmax from $\log(\pi)$. In practice, this method has been shown to suffer from unstable optimization behavior.

2.3. Other methods

While methods such as SGA aim to optimize the latent variables for neural image compression at inference time, other approaches have been explored in recent research. (Guo et al., 2021) proposed a soft-then-hard strategy alongside a learned scaling factor for the uniform noise to achieve better compression and a smoother latent. These methods are used to fine-tune network parameters but not the latents directly. (Zhu et al., 2022) proposed using Swin-transformer-based coding instead of ConvNet-based coding. They showed that these transforms can achieve better compression with fewer parameters and shorter decoding times. (van Rozendaal et al., 2021) proposed to also fine-tune the decoder alongside

the latent for video compression. While accommodating the additional cost of saving the model update, they demonstrated a gain of $\sim 1dB$. (Zhang et al., 2021) and (Dupont et al., 2021) proposed using implicit neural representations for video and image compression, respectively. (He et al., 2022) proposed an improved context model (SCCTX) and a change to the main transform (ELIC) that achieve strong compression results together. (El-Nouby et al., 2023) revisited vector quantization for neural image compression and demonstrated it performs on par with hyperprior-based methods. While these approaches change the training process, our work differs in that we only consider the inference process.

3. Methods

As literature has shown, refining the latents of pre-trained compression models with SGA leads to improved compression performance (Yang et al., 2020). In this section, we extend SGA by introducing SGA+ containing three other methods for the computation of the unnormalized log probabilities $\log(\pi)$ to overcome issues from its predecessor. We show how these methods behave in probability space. Furthermore, we show how the methods can be extended to three-class rounding.

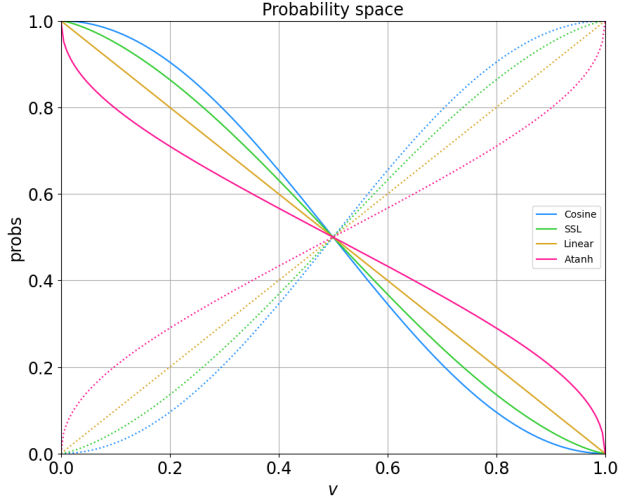
3.1. Two-class rounding

Recall from SGA that a variable v is quantized to indicate the rounding direction to two classes and is centered between $(0,1)$. Computation of the unnormalized log probabilities is obtained with atanh from Equation (3). When looking at the probability space from this function, see Figure 1a, the atanh function can lead to sub-optimal performance when used to determine rounding probabilities. The problem is that gradients tend to infinity when the function approaches the limits of 0 and 1. This is not ideal, as these limits are usually achieved when the discretization gap is minimal. In addition, the gradients may become larger towards the end of optimization. Further analyzing the probability space, we find that there are a lot of possibilities in choosing probabilities for rounding to two classes. However, there are some constraints: the probabilities need to be monotonic functions, and the probabilities for rounding down (flooring) and up (ceiling) need to sum up to one. Therefore, we introduce SGA+ and propose three methods that satisfy the above constraints and can be used to overcome the sub-optimality that the atanh function suffers from.

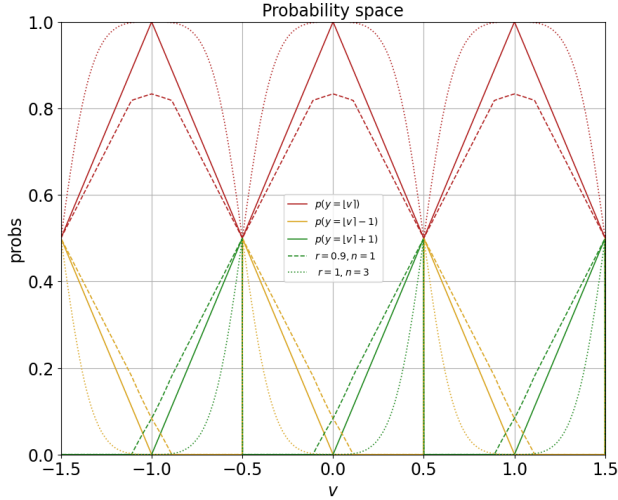
We will denote the probability that v is rounded down by:

$$p(y = \lfloor v \rfloor), \quad (4)$$

where y represents the random variable whose outcome can be either rounded down or up. The probability that v is



(a) The probability space for different functions of SGA+: linear, cosine and SSL ($a = \frac{4}{3}$), along with atanh. Solid lines denote the probability of flooring $\lfloor v \rfloor$ and dotted lines the probability of ceiling $\lceil v \rceil$.



(b) Three-class rounding for the extended version of linear. Solid lines denote the two-class rounding with $r = 1$ and $n = 1$. Dashed lines denote three-class rounding with $r = 0.9$ and $n = 1$ and the dotted lines indicate the smoothness for $r = 1$ and $n = 3$.

Figure 1. Probability space for (a) Two-class rounding (b) Three-class rounding

rounded up is conversely: $p(y = \lceil v \rceil) = 1 - p(y = \lfloor v \rfloor)$.

Linear probabilities To prevent gradient saturation or vanishing gradients completely, the most natural case would be to model a probability that linearly increases or decreases and has a gradient of one everywhere. Therefore, we define the linear:

$$p(y = \lfloor v \rfloor) = 1 - (v - \lfloor v \rfloor). \quad (5)$$

It is easy to see that: $p(y = \lceil v \rceil) = v - \lfloor v \rfloor$. In Figure 1a, the linear probability is shown.

Cosine probabilities As can be seen in Figure 1a, the atanh tends to have gradients that go to infinity for v close to the corners. Subsequently, a method that has low gradients in that area is by modeling the cosine probability as follows:

$$p(y = \lfloor v \rfloor) = \cos^2 \left(\frac{(v - \lfloor v \rfloor)\pi}{2} \right). \quad (6)$$

This method aids the compression performance compared to the atanh since there is less probability of overshooting the rounding value.

Sigmoid scaled logit There are a lot of possibilities in choosing probabilities for two-class rounding. We introduced two probabilities that overcome sub-optimality issues from atanh: the linear probability from Equation (5), which has equal gradients everywhere, and cosine from Equation (6), that has little gradients at the corners. Besides these two functions, the optimal probability might follow a different function from the ones already mentioned. Therefore, we introduce the sigmoid scaled logit (SSL), which can interpolate between different probabilities with its hyperparameter a and is defined as follows:

$$p(y = \lfloor v \rfloor) = \sigma(-a\sigma^{-1}(v - \lfloor v \rfloor)), \quad (7)$$

where a is the factor determining the shape of the function. SSL resembles exactly the linear for $a = 1$. For $a = 1.6$ and $a = 0.65$ SSL roughly resembles the cosine and atanh. For $a \rightarrow \infty$ the function tends to shape to (reversed) rounding.

3.2. Three-class rounding

As described in the previous section, the values for v can either be floored or ceiled. However, there are cases where it may help to round to an integer further away. Therefore, we introduce three-class rounding and show three extensions that build on top of the linear probability Equation (5), cosine probability Equation (6), and SSL from Equation (7).

The probability that v is rounded is denoted by: $p(y = \lfloor v \rfloor) \propto f_{3c}(w|r, n)$, where $w = v - \lfloor v \rfloor$ is centered around zero. Further, we define the probability that v is rounded +1 and rounded -1 is respectively given by: $p(y = \lfloor v \rfloor - 1) \propto f_{3c}(w-1|r, n)$ and $p(y = \lfloor v \rfloor + 1) \propto f_{3c}(w+1|r, n)$. The general notation for the three-class functions is given by:

$$f_{3c}(w|r, n) = f(\text{clip}(w \cdot r))^n, \quad (8)$$

where $\text{clip}(\cdot)$ clips the value at 0 and 1, r is the factor determining the height and steepness of the function and power n controls the peakedness of the function.

Extended linear Recall that the linear probability can now be extended to three-class rounding as follows:

$$f_{linear}(w) = |w|. \quad (9)$$

A special case is $f_{3c,linear}(w|r = 1, n = 1)$, where the function is equivalent to the linear of the two-class rounding from Equation (5). For $r < 1$ this function rounds to three classes, and for $n \neq 1$ this function is not linear anymore.

In Figure 1b, the three-class rounding for the extension of Equation (5) can be found. As can be seen, the solid lines denote the special case of two-class rounding with $r = 1$ and $n = 1$, the dashed lines denote three-class rounding with $r = 0.9$ and $n = 1$ and the dotted lines denote the two-class rounding with $r = 1$ and $n = 3$, which shows a less peaked function. We can now compare an example of two- versus three-class rounding. Consider the case where we have variable $v = -0.95$. For two-class rounding there is only the chance of rounding to -1 with $p(y = \lfloor v \rfloor)$ (red solid line), a chance to round to 0 with $p(y = \lfloor v \rfloor + 1)$ (green solid line) and zero chance to round to -2 with $p(y = \lfloor v \rfloor - 1)$ (yellow solid line). Now for three-class rounding, with $r = 0.9$ and $n = 1$, when $v = -0.95$ we find that there is a high chance to round to -1 with $p(y = \lfloor v \rfloor)$ (red dashed line) and a small chance to round to 0 with $p(y = \lfloor v \rfloor + 1)$ (green dashed line) and a tiny chance to round to -2 with $p(y = \lfloor v \rfloor - 1)$ (yellow dashed line).

Extended cosine Similarly, we can transform the cosine probability from Equation (6) to three-class rounding:

$$f_{cosine}(w) = \cos\left(\frac{|w|\pi}{2}\right). \quad (10)$$

When $f_{3c,cosine}(w|r = 1, n = 2)$, this function exactly resembles the cosine for two-class rounding, and for $r < 1$ this function rounds to three classes.

Extended SSL Additionally, SSL from Equation (7) can be transformed to three-class rounding as follows:

$$f_{SSL}(w) = \sigma(-a\sigma^{-1}(|w|)), \quad (11)$$

where a is the factor determining the shape of the function. When $f_{3c,SSL}(w|r = 1, n = 1)$, this function exactly resembles the two-class rounding case, and for $r < 1$, the function rounds to three classes. Recall that this function is capable of exactly resembling the linear function and approximates the cosine from two-class rounding for $a = 1$ and $a = 1.6$, respectively.

4. Experiments

In this section, we evaluate our best-performing method and compare it to the baselines with the true R-D loss performance ($\hat{\mathcal{L}}$), the difference between the method loss and true

loss ($\mathcal{L} - \hat{\mathcal{L}}$), and corresponding PSNR and BPP plot that respectively expresses the image quality, and cost over t training steps. Next, an in-depth analysis of the stability of each proposed method is shown, followed by an experiment that expresses changes in the true R-D loss performance when one interpolates between functions. Additionally, we evaluate the three-class rounding for each of the proposed methods. Finally, we show how our best-performing method performs on the Tecnick dataset and how the method can be deployed to partly move along the rate-distortion curve.

Following (Yang et al., 2020), we run all experiments with temperature schedule $\tau(t) = \min(\exp\{-ct\}, \tau_{max})$, where c is the temperature rate determining how fast temperature τ is decreasing over time, t is the number of train steps for the refinement of the latents and $\tau_{max} \in (0, 1)$ determines how soft the latents start the refining procedure. Additionally, we refine the latents for $t = 2000$ train iterations, unless specified otherwise. For more hyperparameter settings, see Section 4.6. Further, the experimental results are obtained from a pre-trained model trained with $\lambda = 0.01$.

4.1. Implementation details

The pre-trained mean-scale hyperpriors are trained from scratch on the full-size CLIC 2020 Mobile dataset (Toderici et al., 2020), mixed with the ImageNet 2012 dataset (Rusakovsky et al., 2015) with randomly cropped image patches taken of size 256×256 . For ImageNet, only images with a size larger than 256 for height and width are used to prevent bilinear up-sampling that negatively affects the model performance. We use the architecture of (Minnen et al., 2018), except for the autoregressive part as a context model. Instead, we use the regular convolutional architecture of (Ballé et al., 2018). The model package for the mean-scale hyperprior is from CompressAI (Bégaint et al., 2020). During training, each model is evaluated on the Kodak dataset (Kodak). We run all models and methods on a single NVIDIA A100 GPU.

The models are trained with $\lambda = \{0.001, 0.0025, 0.005, 0.01, 0.02, 0.04, 0.08\}$, with a batch size of 32 and Adam optimizer with a learning rate set to $1e^{-4}$. The models are trained for 2M steps, except for model $\lambda = 0.001$, which is trained for 1M steps and model $\lambda = 0.08$, which is trained for 3M steps. Further, the models for $\lambda = \{0.04, 0.08\}$ are trained with 256 hidden channels and the model for $\lambda = 0.001$ is trained with 128 hidden channels. The remaining models are trained with hidden channels set to 192.

4.2. Baseline methods

We compare our methods against the methods that already exist in the literature. The **Straight-Through Estimator** (STE) is a method to round up or down to the nearest integer with a rounding bound set to a half. This rounding is noted

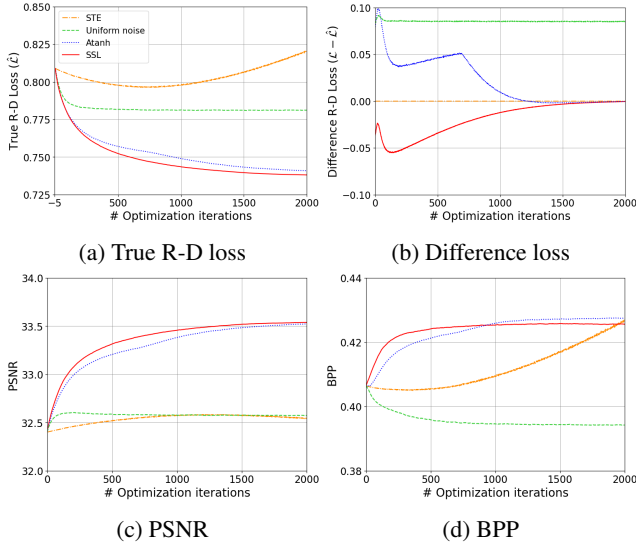


Figure 2. Performance plots of (a) True R-D Loss (b) Difference in loss (c) PSNR (d) BPP

as $[\cdot]$. The derivative of STE for the backward pass is equal to 1 (Bengio et al., 2013; Van Den Oord et al., 2017; Yin et al., 2019). The **Uniform Noise** quantization method adds uniform noise from $u \sim U(-\frac{1}{2}, \frac{1}{2})$ to latent variable y . Thus: $\hat{y} = y + u$. In this manner \hat{y} becomes differentiable (Ballé et al., 2017). As discussed in Section 2.2, we compare against **Stochastic Gumbel Annealing**, which is a soft-to-hard quantization method that quantizes a continuous variable v into a discrete representation for which gradients can be computed.

4.3. Experimental results

Overall performance Figure 2 shows the overall performance for the refinement of the latents on the Kodak dataset with method: STE, uniform noise, atanh and SSL. The true R-D loss in Figure 2a shows that STE has trouble converging and uniform noise quickly converges compared to atanh and SSL. We find that SSL outperforms all other methods, including atanh in terms of the lowest true R-D loss. Looking at the difference between the method loss and true loss Figure 2b, we find that SSL quickly and smoothly finds a balance between the method and true loss, while atanh has a big difference in the beginning and more peaks before eventually converging. Additionally, uniform noise shows a big difference between the method loss and true loss, indicating that adding uniform noise overestimates its method loss compared to the true loss. For R-D curves, we refer to Appendix A.2.

Temperature sensitivity Now that we have assessed the overall performance, we analyze the stability of each method. Table 1 represents the stability of atanh and

Table 1. True R-D loss for different τ_{max} settings of: atanh(v), linear, cosine and SSL with $a = \frac{4}{3}$. Lowest R-D loss per column is marked with: \downarrow . Note that the function containing atanh is unnormalized.

Function \ τ_{max}	0.2	0.4	0.6	0.8	1.0
exp atanh(v)	0.7445 \downarrow	0.7408	0.7412	0.7416	0.7418
$1 - v$ (linear)	0.7458	0.7406 \downarrow	0.7390 \downarrow	0.7386	0.7386
$\cos^2(\frac{v\pi}{2})$	0.7496	0.7414	0.7393	0.7387	0.7384
$\sigma(-a\sigma^{-1}(v))$	0.7578	0.7409	0.7391	0.7383 \downarrow	0.7380 \downarrow
exp atanh(v)	0	0.0002	0.0022	0.0033	0.0038
$1 - v$ (linear)	0.0013	0	0	0.0003	0.0006

the SGA+ methods, expressed in true R-D loss, for different τ_{max} settings for the temperature schedule. As can be seen, the most optimal setting is with $\tau_{max} = 1$ for each of the SGA+ methods. atanh obtains equal loss for $\tau_{max} \in [0.4, 0.5]$. In general, we find that the linear method of SGA+ is least sensitive to changes in τ_{max} and has equal loss between $\tau_{max} \in [0.7, 1]$. To further examine the stability of the linear function compared to atanh, we subtract the best τ_{max} , column-wise, from the linear and atanh of that column. We now see that the linear function is not only least sensitive to changes in τ_{max} , but overall varies little compared to the best τ_{max} settings of the other methods. While the SSL has the largest drop in performance when reducing τ_{max} , it achieves the highest performance overall for higher values of τ_{max} .

Table 2. True R-D loss results for the interpolation between different functions by changing a of the SSL.

a	R-D Loss
0.01	1.15
0.3	0.7528
0.65 (approx atanh)	0.7410
0.8	0.7396
1 (linear)	0.7386
1.33	0.7380 \downarrow
1.6 (approx cosine)	0.7382
2.25	0.7388
5	0.7415

Interpolation Table 2 represents the interpolation between different functions, expressed in true R-D loss. Values for $a < 1$ indicate methods that tend to have (extremely) large gradients for v close to the corners, while high values of a represent a method that tends to a (reversed) step function. We find that SLL with small $a = \{0.01, 0.3\}$ diverges and results in large loss values compared to the rest. Additionally, the loss curves show unstable behavior for these functions, which can be found in Appendix A.1. For $a = \{0.8, \dots, 2.25\}$, the loss shows stable behavior in terms of its curves and final loss at $t = 2000$. Furthermore, for $a = 1.65$ (approximately atanh), the method shows

non-optimal behavior due to a slightly unstable loss curve, see Appendix A.1, this may be due to setting $\tau_{max} = 1$ instead of optimal setting $\tau_{max} = [0.4, 0.5]$. Note that the difference in loss 0.7410 for SSL $a = 0.65$ and 0.7418 for atanh with $\tau_{max} = 1$ (see Table 1). This difference may be because SSL is an approximation to the atanh function and not exactly equal.

Three-class rounding In Table 3, the true R-D loss for two versus three-class rounding can be found at iteration $t = 500$ and in brackets $t = 2000$ iterations. For each method, we performed a grid search over the hyperparameters r and n . Additionally, for the extended SSL, we also performed a grid search over a and found the best setting to be $a = 1.4$. As can be seen in the table, most impact is made with the extended version of the linear of SGA+, in terms of the difference between the two versus three-class rounding at iteration $t = 500$ with loss difference 0.0035 and $t = 2000$ with 0.0006 difference. There is a small difference at $t = 500$ for the extended cosine version. In general, we find that running models longer results in convergence to similar values. SSL converges to equal values for two- and three-class rounding. This makes three-class rounding attractive under a constraint optimization budget, possibly because it is easier to jump between classes.

Table 3. True R-D loss of two versus three-class rounding for SGA+ with the extended version of the linear, cosine, and SSL method at iteration 500 and in brackets after 2000 iterations.

Function \ Rounding	Two	Three
$f_{3c,linear}(w r = 0.98, n = 1.5)$	0.7552 (0.7386)	0.7517(0.7380)
$f_{3c,cosine}(w r = 0.98, n = 2)$	0.7512 (0.7384)	0.7513 (0.7379)
$f_{3c,sigmoidlogit}(w r = 0.93, n = 1.5)$	0.7524 (0.7380)	0.7504 (0.7380)

4.4. Tecnick

To test how our method performs on another dataset, we use the Tecnick dataset (Asuni & Giachetti, 2014). We run baselines atanh and the base model and compare against SSL with $a = \frac{4}{3}$. Figure 3 shows the corresponding R-D curves, using image quality metric PSNR versus BPP, after $t = 500$ iterations. We find that both refining methods greatly improve the compression performance in terms of the R-D trade-off. Additionally, our proposed method outperforms the baselines and shows how it boosts performance, especially for the smallest and highest $\lambda = \{0.001, 0.08\}$. The R-D plot after $t = 2000$ iterations can be found in Appendix A.2.

4.5. Semi-multi-rate behavior

An interesting observation is that one does not need to use the same λ during refinement of the latents, as used during training. As a consequence of this approach, we can

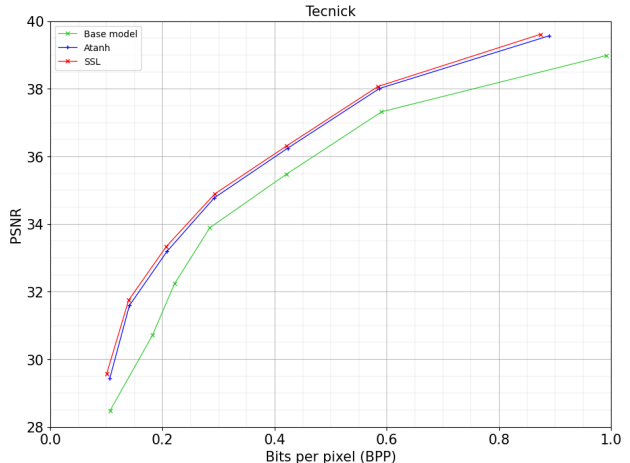


Figure 3. Rate-distortion performance on the Tecnick dataset at iteration 500 for the base model, atanh and SSL.

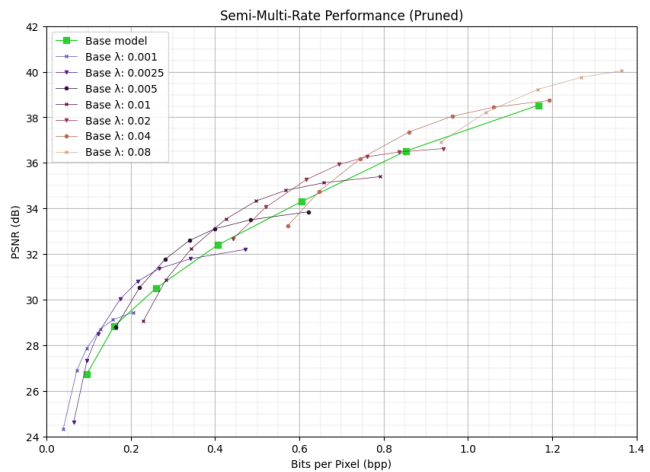


Figure 4. RD-plot with semi-multi-rate behavior.

optimize to a neighborhood of the R-D curve without the need to train a new model from scratch. For instance, we only need three out of seven models to have better performance over the entire curve compared to the base model. We experimented with different values for λ . For every pre-trained model, we ran our best SSL approach using $\lambda \in \{0.0001, 0.0005, 0.001, 0.0025, 0.005, 0.01, 0.02, 0.04, 0.08, 0.16, 0.32\}$ to obtain a semi-multi-rate curve. In Figure 4, we have plotted the R-D curve of the base model (lime green line) and its corresponding R-D curves, obtained when refining the latents with the proposed λ 's. We pruned away points that fell too far below the base curve and refer to Appendix A.3 for the unpruned version.

Qualitative results In Figure 5, we demonstrate the effects of using the semi-multi-rate strategy. We compare the original image, the compressed image using the base model for $\lambda = 0.001$, and the compressed image using SSL

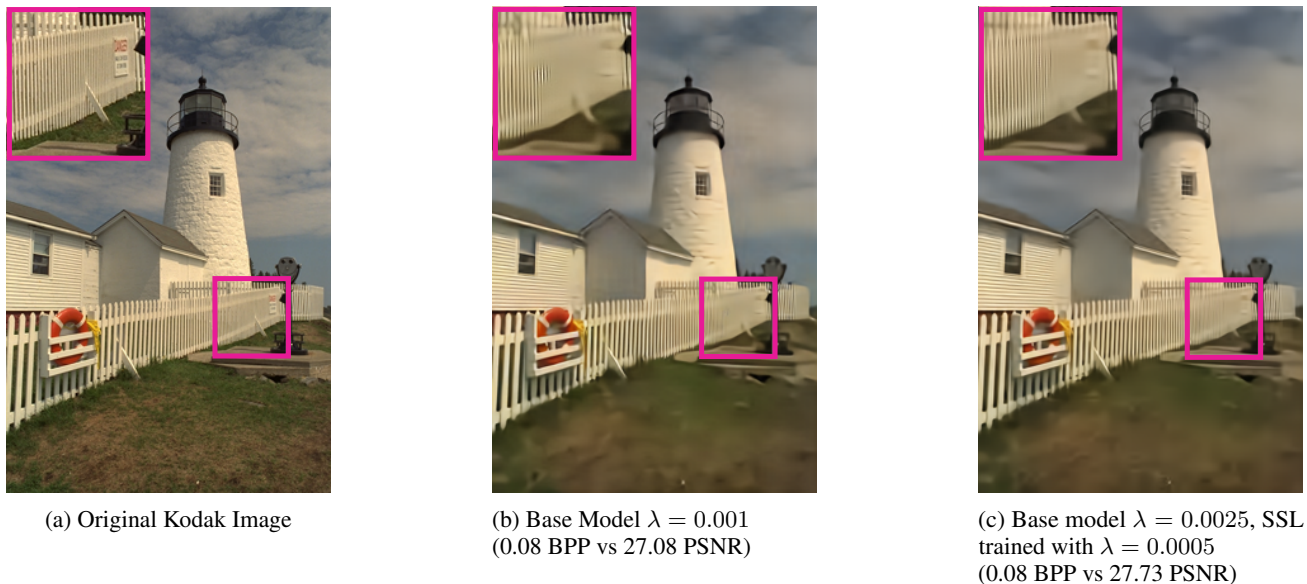


Figure 5. Qualitative comparison of an Kodak image which can be best viewed electronically. Base model for $\lambda = 0.001$ compared to base model $\lambda = 0.0025$ tuned with $\lambda = 0.0005$ during the refinement procedure for SSL.

with a base $\lambda = 0.0025$ and a target $\lambda = 0.0005$. We have chosen the latter two to compare as their BPP values are similar, while the base models are different. For the image compressed by SSL, we observe that there are less artifacts visible. For instance, looking at the fence we see more texture compared to the base model. Additionally, looking at the sky we find less artifacts compared to the base model.

4.6. Hyperparameter settings

Similar to (Yang et al., 2020), we find an optimal learning rate of 0.005 for atanh and find the best performance for STE with a smaller learning rate of 0.0001, yet STE still has trouble converging. Additionally, we find the best performance for atanh with $\tau_{max} \in [0.4, 0.5]$. For SGA+, we use optimal convergence settings, which are a fixed learning rate of 0.005, a temperature rate of $c = 0.001$, and $\tau_{max} = 1$. Furthermore, experimentally, we find approximately equal and best performance for SLL with $a \in [1.3, 1.4]$. For SSL we choose $a = \frac{4}{3}$, see corresponding probability in Figure 1a.

5. Discussion and conclusion

Training neural image compression models is a time-consuming and difficult task. In practice, finding optimal encoding comes with difficulties and can lead to sub-optimal performance of these networks. Refining latents of a pre-trained network has been shown to improve the compression performance by adding uniform noise or using a stochastic method called SGA (Campos et al., 2019; Yang et al., 2020).

We extend this idea and propose SGA+. We show how SGA+ has nicer properties, which aids the compression performance. We introduced SSL that can approximately interpolate between all of the proposed methods. Further, we show how our best-performing method SSL outperforms the baselines and that it is more stable under varying conditions. We give a general notation and demonstrate how the extension to three-class rounding improves the convergence of the SGA+ methods but comes with the cost of fine-tuning extra hyperparameters. Finally, we show how our proposed method performs when refining latents on the Tecnick dataset and how we can use refining of the latents to obtain semi-multi-rate behavior.

In general, it applies for each method that as the temperature rate has reached a stable setting, the longer you train, the closer together the performance will be. However, when under a constrained optimization budget, running SGA+ shorter already gives good results. The best results are obtained while tuning the hyperparameter of SSL. Further, our experiments show that the linear version for SGA+ is least sensitive to hyperparameter changes.

Broader impact

The development and improvement of neural compression techniques play an important role in our increasingly data-driven society. Being able to learn compression codecs as opposed to developing them saves time and effort. There is a rich array of signal-based data types available that benefit from compression. A smaller data footprint reduces the requirements for storage, networking, and computing resources. It thus also means smaller investments in terms of raw resources, manufacturing, energy, and labor.

Neural image compression methods still require a large amount of computation to be trained. This process has tremendous adverse effects on the environment, as established earlier. Our work aims to make these models more flexible through the proposal of methods that improve on these already trained models. Improved flexibility can result in improved reusability, which may reduce the environmental impact of neural image codecs.

References

- Agustsson, E., Mentzer, F., Tschannen, M., Cavigelli, L., Timofte, R., Benini, L., and Gool, L. V. Soft-to-hard vector quantization for end-to-end learning compressible representations. *Advances in neural information processing systems*, 30, 2017.
- Agustsson, E., Minnen, D., Johnston, N., Balle, J., Hwang, S. J., and Toderici, G. Scale-space flow for end-to-end optimized video compression. In *IEEE conference on Computer Vision and Pattern Recognition*, 2020.
- Asuni, N. and Giachetti, A. TESTIMAGES: A large-scale archive for testing visual devices and basic image processing algorithms (SAMPLING 1200 RGB set). In *STAG: Smart Tools and Apps for Graphics*, 2014. URL https://sourceforge.net/projects/testimages/files/OLD/OLD_SAMPLING/testimages.zip.
- Aytekin, C., Ni, X., Cricri, F., Lainema, J., Aksu, E., and Hannuksela, M. Block-optimized variable bit rate neural image compression. In *Proceedings of the IEEE Conference on Computer Vision and Pattern Recognition Workshops*, pp. 2551–2554, 2018.
- Ballé, J., Laparra, V., and Simoncelli, E. P. End-to-end optimized image compression. *International Conference on Learning Representations*, 2017.
- Ballé, J., Minnen, D., Singh, S., Hwang, S. J., and Johnston, N. Variational image compression with a scale hyperprior. *arXiv preprint arXiv:1802.01436*, 2018.
- Bégaint, J., Racapé, F., Feltman, S., and Pushparaja, A. Compressai: a pytorch library and evaluation platform for end-to-end compression research. *arXiv preprint arXiv:2011.03029*, 2020.
- Bellard, F. BPG specification, 2014. URL https://bellard.org/bpg/bpg_spec.txt. (accessed June 3, 2020).
- Bengio, Y., Léonard, N., and Courville, A. Estimating or propagating gradients through stochastic neurons for conditional computation. *arXiv preprint arXiv:1308.3432*, 2013.
- Campos, J., Meierhans, S., Djelouah, A., and Schroers, C. Content adaptive optimization for neural image compression. *arXiv preprint arXiv:1906.01223*, 2019.
- Cremer, C., Li, X., and Duvenaud, D. Inference suboptimality in variational autoencoders. In *International Conference on Machine Learning*, pp. 1078–1086. PMLR, 2018.
- Dupont, E., Golinski, A., Alizadeh, M., Teh, Y. W., and Doucet, A. COIN: compression with implicit neural representations. *CoRR*, abs/2103.03123, 2021.
- El-Nouby, A., Muckley, M. J., Ullrich, K., Laptev, I., Verbeek, J., and Jégou, H. Image compression with product quantized masked image modeling. *Trans. Mach. Learn. Res.*, 2023, 2023.
- Guo, T., Wang, J., Cui, Z., Feng, Y., Ge, Y., and Bai, B. Variable rate image compression with content adaptive optimization. In *Proceedings of the IEEE/CVF Conference on Computer Vision and Pattern Recognition Workshops*, pp. 122–123, 2020.
- Guo, Z., Zhang, Z., Feng, R., and Chen, Z. Soft then hard: Rethinking the quantization in neural image compression. In Meila, M. and Zhang, T. (eds.), *Proceedings of the 38th International Conference on Machine Learning*, volume 139 of *Proceedings of Machine Learning Research*, pp. 3920–3929. PMLR, 18–24 Jul 2021.
- Habibian, A., Rozendaal, T. v., Tomczak, J. M., and Cohen, T. S. Video compression with rate-distortion autoencoders. In *IEEE International Conference on Computer Vision*, 2019.
- He, D., Yang, Z., Peng, W., Ma, R., Qin, H., and Wang, Y. ELIC: efficient learned image compression with unevenly grouped space-channel contextual adaptive coding. In *IEEE/CVF Conference on Computer Vision and Pattern Recognition, CVPR 2022, New Orleans, LA, USA, June 18-24, 2022*, pp. 5708–5717. IEEE, 2022. doi: 10.1109/CVPR52688.2022.00563.
- Jang, E., Gu, S., and Poole, B. Categorical reparameterization with gumbel-softmax. *arXiv preprint arXiv:1611.01144*, 2016.

- Kingma, D. P. and Welling, M. Auto-encoding variational bayes. *arXiv preprint arXiv:1312.6114*, 2013.
- Kodak, E. Kodak lossless true color image suite (PhotoCD PCD0992). URL <http://r0k.us/graphics/kodak>.
- Lee, J., Cho, S., and Beack, S.-K. Context-adaptive entropy model for end-to-end optimized image compression. In *the 7th Int. Conf. on Learning Representations*, May 2019.
- Lu, G., Ouyang, W., Xu, D., Zhang, X., Cai, C., and Gao, Z. Dvc: An end-to-end deep video compression framework. In *IEEE conference on Computer Vision and Pattern Recognition*, 2019.
- Lu, G., Cai, C., Zhang, X., Chen, L., Ouyang, W., Xu, D., and Gao, Z. Content adaptive and error propagation aware deep video compression. In *Computer Vision—ECCV 2020: 16th European Conference, Glasgow, UK, August 23–28, 2020, Proceedings, Part II 16*, pp. 456–472. Springer, 2020.
- Minnen, D., Ballé, J., and Toderici, G. D. Joint autoregressive and hierarchical priors for learned image compression. *Advances in neural information processing systems*, 31, 2018.
- Russakovsky, O., Deng, J., Su, H., Krause, J., Satheesh, S., Ma, S., Huang, Z., Karpathy, A., Khosla, A., Bernstein, M., Berg, A. C., and Fei-Fei, L. ImageNet Large Scale Visual Recognition Challenge. *International Journal of Computer Vision (IJCV)*, 115(3):211–252, 2015. doi: 10.1007/s11263-015-0816-y.
- Skodras, A., Christopoulos, C., and Ebrahimi, T. The jpeg 2000 still image compression standard. *IEEE Signal Processing Magazine*, 2001.
- Theis, L., Shi, W., Cunningham, A., and Huszár, F. Lossy image compression with compressive autoencoders. *arXiv preprint arXiv:1703.00395*, 2017.
- Toderici, G., Vincent, D., Johnston, N., Jin Hwang, S., Minnen, D., Shor, J., and Covell, M. Full resolution image compression with recurrent neural networks. In *Proceedings of the IEEE conference on Computer Vision and Pattern Recognition*, pp. 5306–5314, 2017.
- Toderici, G., Shi, W., Timofte, R., Theis, L., Balle, J., Agustsson, E., Johnston, N., and Mentzer, F. Workshop and challenge on learned image compression (clic2020), 2020. URL <http://www.compression.cc>.
- Van Den Oord, A., Vinyals, O., et al. Neural discrete representation learning. *Advances in neural information processing systems*, 30, 2017.
- van Rozendaal, T., Huijben, I. A. M., and Cohen, T. Overfitting for fun and profit: Instance-adaptive data compression. In *9th International Conference on Learning Representations, ICLR 2021, Virtual Event, Austria, May 3-7, 2021*. OpenReview.net, 2021.
- Wallace, G. K. The jpeg still picture compression standard. *IEEE transactions on consumer electronics*, 38(1):xviii–xxxiv, 1992.
- Yang, Y., Bamler, R., and Mandt, S. Improving inference for neural image compression. *Advances in Neural Information Processing Systems*, 33:573–584, 2020.
- Yin, P., Lyu, J., Zhang, S., Osher, S., Qi, Y., and Xin, J. Understanding straight-through estimator in training activation quantized neural nets. *arXiv preprint arXiv:1903.05662*, 2019.
- Zhang, Y., van Rozendaal, T., Brehmer, J., Nagel, M., and Cohen, T. Implicit neural video compression. *CoRR*, abs/2112.11312, 2021.
- Zhu, Y., Yang, Y., and Cohen, T. Transformer-based transform coding. In *The Tenth International Conference on Learning Representations, ICLR 2022, Virtual Event, April 25-29, 2022*. OpenReview.net, 2022.

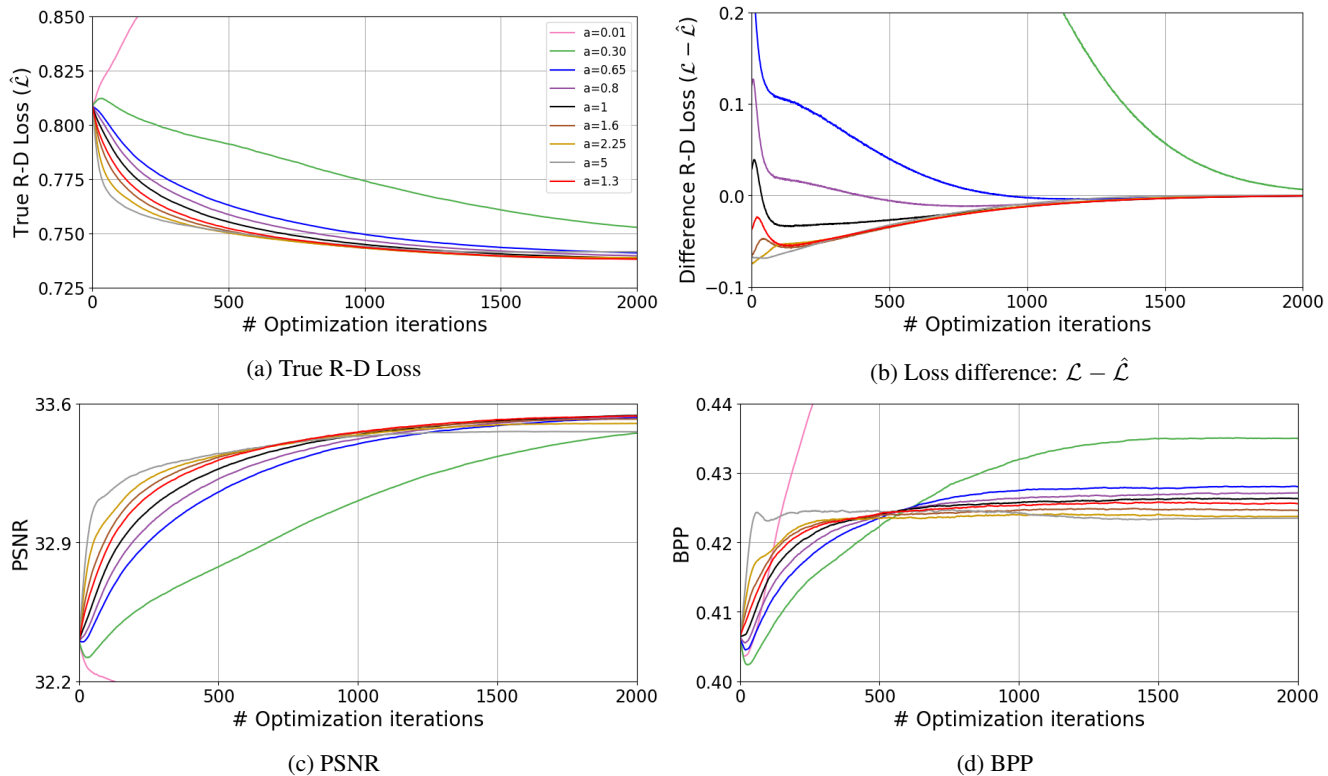


Figure 6. Interpolation performance plots of different a settings for SLL (a) True R-D Loss (b) Difference in loss (c) PSNR (d) BPP

A. Additional results

In this appendix, additional experiment results can be found.

A.1. Interpolation

Table 2 presents the true R-D loss results for the interpolation with different a settings for SSL. In Figure 6, the corresponding overall performance of the methods can be found. As can be seen in Figure 6a, for $a = \{0.01, 0.30\}$, the functions diverge, resulting in large loss values. For $a = 0.65$, we find that the loss curve is slightly unstable at the beginning of training, which can be seen in the bending of the curve, indicating non-optimal settings. This may be due to the fact that we run all methods with the same $\tau_{max} = 1$ for a fair comparison. Additionally, note that SSL with $a = 0.65$ obtains a true R-D loss of 0.7410 compared to 0.7418 for atanh with the same settings. This is due to the fact that SSL, especially in the tails of the probability, is slightly more straight-curved compared to the atanh when looking at its probability space.

Remarkably, for $a \geq 1$, the difference in losses start close to zero (see Figure 6b). SSL with $a = 5$ results in the fastest convergence and quickly finds a stable point but ends at a higher loss than most methods.

A.2. Rate-Distortion performance

We evaluate our best performing method SSL with $a = \frac{4}{3}$ on the Kodak and Tecnick datasets, by computing the R-D performance, average over each of the datasets. The R-D curves use image quality metric PSNR versus BPP on the Kodak and Tecnick dataset. Recall that as base model we use the pre-trained mean-scale hyperprior, trained with $\lambda = \{0.001, 0.0025, 0.005, 0.01, 0.02, 0.04, 0.08\}$.

Kodak Figure 7 shows the R-D curve for refining the latents, evaluated on Kodak. We compare SLL against baselines: STE, uniform noise, atanh and the base model at iteration $t = 500$ (see Figure 7a) and after full convergence at $t = 2000$ (see Figure 7b). As can be seen in Figure 7a, STE performs slightly better than the base model, while after $t = 2000$ iterations the method performs worse, this also reflected in the corresponding true loss curve for $\lambda = 0.01$ (see Figure 2a),

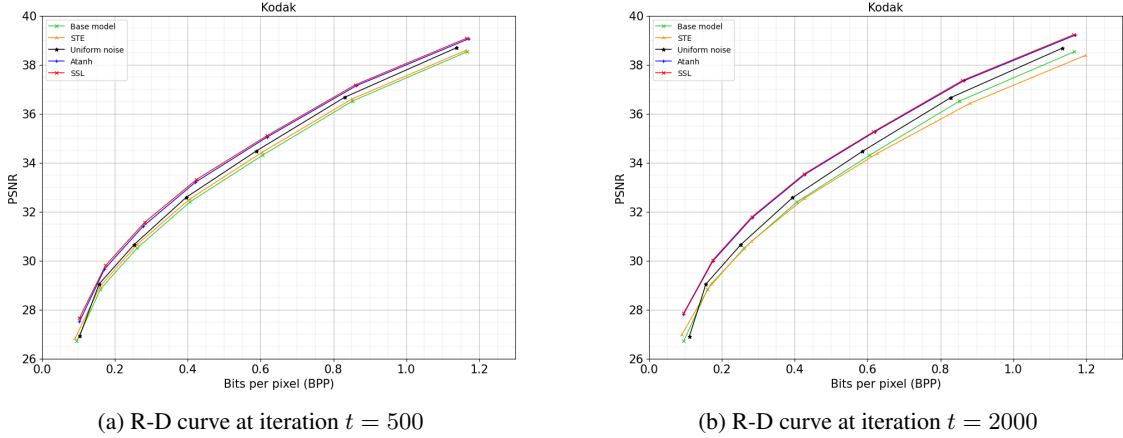


Figure 7. R-D performance on Kodak of the base model, STE, Uniform noise, SGA atanh and SSL with $a = \frac{4}{3}$

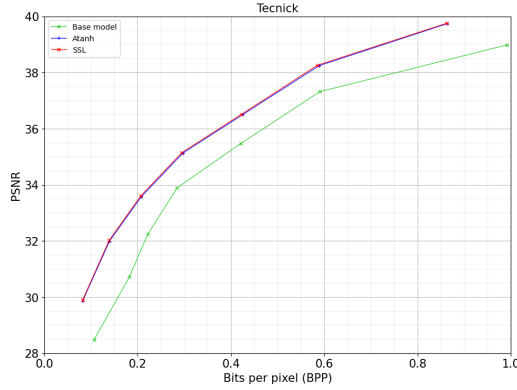


Figure 8. R-D performance on Tecnick after $t = 2000$ iterations, which compares SSL with the baselines: base model and atanh.

which diverges. Remarkably, for the smallest $\lambda = 0.001$, STE performs better than at $t = 500$. Adding uniform noise results in better performance when running the method longer. Further, SSL outperforms atanh slightly, while the difference is more pronounced when running for $t = 500$ iterations.

Tecnick Figure 8 shows the R-D curve when refining latents on the Tecnick dataset, after $t = 2000$ iterations. As can be seen in the plot, we find that the longer the methods run, the closer the performance lies to each other. When there is a limited budget available, one can run the refinement process for $t = 500$ iterations.

A.3. Semi multi-rate behavior

Figure 9 shows the different R-D curves when refining the latents using different values for λ . For each model trained using $\lambda \in \{0.001, 0.0025, 0.005, 0.01, 0.02, 0.04, 0.08\}$, we run SSL with $a = \frac{4}{3}$ for $t = 2000$ iterations for all $\lambda \in \{0.0001, 0.0005, 0.001, 0.0025, 0.005, 0.01, 0.02, 0.04, 0.08, 0.16, 0.32\}$. We depicted the base curve alongside the curves for each base model. We observe that using SGA+ in this manner gives samples diverse enough such that there is always a point on the resulting curve that is better than the base curve. As a result, latent fine-tuning allows for semi-multi-rate behavior. We also observed that when the values for λ used between training and SGA+ differ too much, the resulting BPP versus PSNR point becomes worse than the base model.

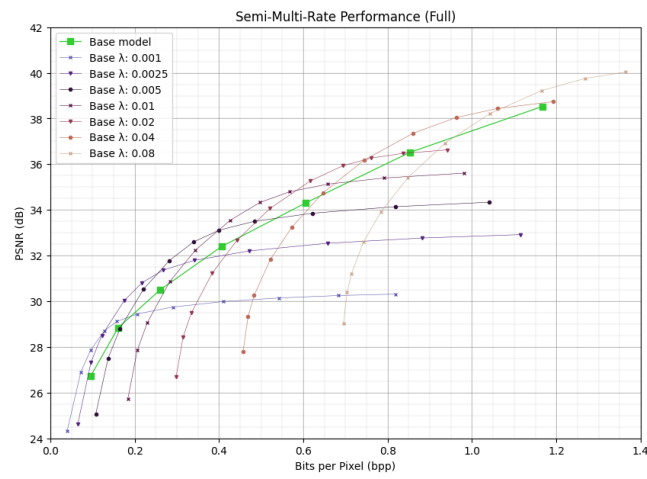


Figure 9. R-D performance with semi-multi-rate behavior. For each base model, we ran SGA+ with $\lambda \in \{0.0001, 0.0005, \dots, 0.16, 0.32\}$ and depicted the resulting BPP/PSNR point.